Title

Lung microenvironments harbor Mycobacterium tuberculosis phenotypes with distinct treatment responses.

Journal

Antimicrobial Agents and Chemotherapy, 67(9)

Authors

Walter, Nicholas
Ernest, Jackie
Dide-Agossou, Christian
et al.

Publication Date

2023-09-19

DOI

10.1128/aac.00284-23

Peer reviewed

AMERICAN SOCIETY FOR MICROBIOLOGY | Antimicrobial Agents and Chemotherapy

Check for updates

| Antimicrobial Chemotherapy | Full-Length Text

Lung microenvironments harbor *Mycobacterium tuberculosis* phenotypes with distinct treatment responses

Nicholas D. Walter,[1,2,3] Jackie P. Ernest,[4] Christian Dide-Agossou,[1,2] Allison A. Bauman,[5] Michelle E. Ramey,[5] Karen Rossmassler,[1,2] Lisa M. Massoudi,[5] Samantha Pauly,[1,2] Reem Al Mubarak,[1,2] Martin I. Voskuil,[3,6] Firat Kaya,[7] Jansy P. Sarathy,[7] Matthew D. Zimmerman,[7] Véronique Dartois,[7] Brendan K. Podell,[3,5] Radojka M. Savic,[3,4] Gregory T. Robertson[3,5]

AUTHOR AFFILIATIONS See affiliation list on p. 13.

ABSTRACT Tuberculosis lung lesions are complex and harbor heterogeneous microenvironments that influence antibiotic effectiveness. Major strides have been made recently in understanding drug pharmacokinetics in pulmonary lesions, but the bacterial phenotypes that arise under these conditions and their contribution to drug tolerance are poorly understood. A pharmacodynamic marker called the RS ratio® quantifies ongoing rRNA synthesis based on the abundance of newly synthesized precursor rRNA relative to mature structural rRNA. Application of the RS ratio in the C3HeB/FeJ mouse model demonstrated that *Mycobacterium tuberculosis* populations residing in different tissue microenvironments are phenotypically distinct and respond differently to drug treatment with rifampin, isoniazid, or bedaquiline. This work provides a foundational basis required to address how anatomic and pathologic microenvironmental niches may contribute to long treatment duration and drug tolerance during the treatment of human tuberculosis.

KEYWORDS pharmacodynamics, pharmacokinetics, granuloma, tolerance

To address the ongoing global tuberculosis (TB) epidemic, there is a critical need for new shorter, more effective combination antibiotic regimens. Current standard treatments require 6 months for the treatment of drug-susceptible TB and may take years for certain drug-resistant forms of TB. The development of novel regimens that cure TB more rapidly will require a better understanding of how drugs and regimens affect treatment-refractory bacterial populations.

One reason that TB demands prolonged therapy is the complexity and heterogeneity of TB lung lesions (1–3). Lesional microenvironments influence antibiotic effectiveness in two distinct ways. First, the variable architecture and composition of lesions, including differences in vascularization, fibrosis, inflammatory and immune cell infiltration and activation, and caseum formation, affect drug penetration and retention, resulting in drug- and lesion-specific pharmacokinetic (PK) profiles (2, 4–6). Second, variable physiochemical properties, including levels of O_2, CO_2, H^+, carbon and nitrogen sources, micronutrients, and host immune milieu, elicit differing metabolic and stress responses in *Mycobacterium tuberculosis* (*Mtb*), resulting in phenotypically distinct bacterial populations in lesions that tolerate drug exposure differently. For example, *Mtb* in rabbit caseum is largely nonreplicating and exhibits extreme drug tolerance to many drugs (3). A similar dependence of antibiotic effectiveness on lesional phenotypes has been observed in nonhuman primates and marmosets (reviewed in (2)). Antibiotic effectiveness within a lesion depends on both PK (*i.e.*, drugs must reach the pathogen at therapeutically relevant concentrations) and on the *Mtb* phenotype present (*i.e.*, drugs must have activity against the lesion-specific phenotype) (7). While important strides have recently been made in understanding the PK distribution of antituberculosis agents

Editor Kelly E. Dooley, Vanderbilt University Medical Center, Nashville, Tennessee, USA

Address correspondence to Gregory T. Robertson, gregory.robertson@colostate.edu.

N.W.D., M.I.V., and G.T.R. are listed as co-inventors on US patent No. 16/632,310 that pertains to the RS ratio. The remaining authors have no conflicts of interest to declare.

See the funding table on p. 14.

Received 6 March 2023
Accepted 30 June 2023
Published 11 August 2023

into pulmonary lesions in diverse animal models of TB (6, 8, 9), there remains limited knowledge of lesion *Mtb* phenotypes and how these distinct phenotypes may respond differently to drug exposure (10–14).

Drug effects have traditionally been assessed based on colony forming units (CFU) which enumerate the burden of bacteria capable of growing on agar. We recently described the RS ratio (15), an alternative pharmacodynamic (PD) marker that is conceptually distinct from measures of bacterial burden. The RS ratio quantifies a key bacterial cellular process: ongoing rRNA synthesis. rRNA synthesis is fundamentally linked with bacterial replication (16, 17). In the absence of drug treatment, the RS ratio is a proxy for *Mtb* replication (15). We have previously shown that the potency of a regimen in suppressing the RS ratio is associated with shortening time to nonrelapsing cure in mice (15).

Here we used both CFU and the RS ratio to evaluate the effect of three clinically relevant antibiotics in tissue microenvironments of the C3HeB/FeJ (Kramnik) mouse. We demonstrate that, in the absence of treatment, the *Mtb* populations of caseum, airway, remaining lung, and spleen exhibit distinct phenotypes that have a spectrum of ongoing rRNA synthesis. The RS ratio reveals that drugs with diverse mechanisms of action have different effects on *Mtb* microenvironment-specific phenotypes. Collectively, this work demonstrates that advancing beyond the enumeration of bacterial burden to consider the cellular activity of unique *Mtb* phenotypes provides insight into drug effect in lesions and how microenvironmental niches contribute to the long treatment durations required to cure TB.

RESULTS

Pathology of C3HeB/FeJ mouse microenvironments

After 12 wk of infection, the C3HeB/FeJ mice had diverse and complex pathology that enabled the evaluation of four microenvironments analogous to lesions observed in human TB (2, 18, 19). Discrete well-circumscribed granulomas classified as Type I lesions (2, 18, 19), in which the central caseum is bounded by a peripheral rim of enlarged, vacuolated macrophages and an outer ring of fibrosis and compressed alveolar lung tissue, were surgically incised to extract caseum (Fig. 1A and B). The *Mtb* population in caseum is predominantly extracellular (18, 19).

The second microenvironment was remaining lung after removal of Type I lesions. Remaining lung was dominated by nonnecrotic cellular Type III lesions consisting of an admixture of macrophages and lymphocytes with few neutrophils (Fig. 1C and D). The *Mtb* population of remaining lung is predominantly intracellular within macrophages (18, 19).

The third microenvironment was the airway which was sampled via bronchoalveolar lavage (BAL). In contrast to uninfected mice in which airway lavage is dominated by alveolar macrophages and epithelial cells (Fig. 1G), lavage from untreated *Mtb*-infected mice revealed higher proportions of neutrophils and fewer macrophages (Fig. 1H).

The fourth microenvironment was the spleen. Although spleen contains culturable *Mtb,* the pathological response is limited, consisting of microscopic aggregates of macrophages localized within lymphoid white pulp compartments (Fig. 1E and F).

CFU burden and rRNA synthesis prior to drug treatment in key microenvironmental niches

Prior to drug treatment, CFU per gram was highest in caseum with levels at least 2 $\log_{10}$ CFU higher than in remaining lung or spleen (minimum $P < 0.00001$) (Fig. 2A; Table S1). Because it could not be normalized to the gram, CFU in BAL was not directly comparable to tissues. CFU in remaining lung was lower than in caseum but 0.78 $\log_{10}$ CFU higher than in spleen ($P = 0.02$). The RS ratio identified a range of *Mtb* rRNA synthesis rates from lowest in caseum, intermediate in remaining lung and spleen, and highest in airway, indicating distinct microenvironment-specific phenotypes (Fig. 2B). Differences between the RS ratio in each microenvironment were statistically significant (Table S1).

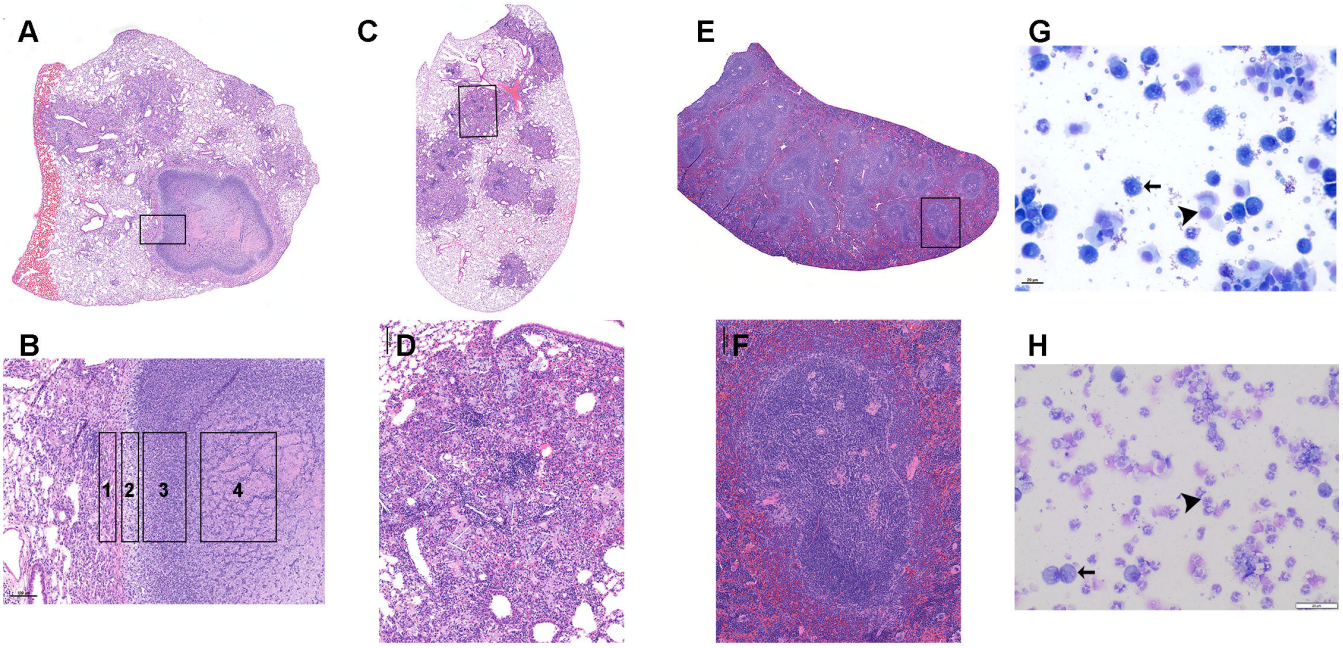

FIG 1 Pathology of four key microenvironments of the C3HeB/FeJ mouse evaluated in this manuscript. The caseum is the central component of the highly organized, caseous necrotic granuloma previously described as a Type I lesion (A and inset shown in B) (2, 18, 19). Type I lesions are bordered by a rim of fibrosis and compressed lung tissue with interstitial inflammation (B, zone 1). Immediately central to the rim is a thin layer of vacuolated macrophages with a high intracellular *Mtb* burden (B, zone 2). The caseum sampled in this study consists of an outer zone of neutrophil-dominated inflammation and an inner zone of cellular debris (B, zone 3 and 4). The caseum is hypoxic, exhibits a near-neutral pH, and contains a high burden of extracellular *Mtb*. The remaining lung is the lung parenchyma remaining after excision of visible Type 1 lesions. The remaining lung consists of Type III lesions (C and inset shown in D), which are cellular non-necrotizing lesions with a relatively low burden of *Mtb* that is intracellular. Spleen (E and inset shown in F) has minimal infection-associated pathology with small aggregates of macrophages contained within the white pulp regions. Airway sampled via bronchoalveolar lavage consists of alveolar macrophages (arrow) and shed airway epithelial cells (arrowhead) in the uninfected animal (G). Following infection, but prior to initiation of treatment, the airway has neutrophil-dominated inflammation (arrowhead) with fewer macrophages (arrow) (H).

Higher CFU was not associated with higher RS ratios. For example, the microenvironment with the highest *Mtb* burden (caseum) had the lowest RS ratio, consistent with a large *Mtb* population and low ongoing rRNA synthesis, suggestive of a slowed bacterial replication rate in caseum. The less concentrated *Mtb* population in remaining lung had an RS ratio sixfold higher than caseum. CFU was similar in the spleen and airway but airway had a significantly higher RS ratio ($P < 0.00001$), suggesting an increased rate of bacterial replication in the oxygen-rich airway. As an additional point of reference, we assayed the RS ratio in the caseum surrogate model (20) used to assess nonspecific caseum drug binding (21, 22) or drug activity against *Mtb* phenotypes that arise after incubation in lipid-rich caseum surrogate (23). The median RS ratio values were 45 in the *ex vivo* caseum surrogate and 33 in caseum from C3HeB/FeJ mice, suggesting the *Mtb* phenotypes are in similar states of rRNA synthesis and replication.

Effect of different drugs in specific microenvironments

Following 2.5 wk of daily treatment, we observed that isoniazid (INH), rifampin (RIF10 or RIF30), and bedaquiline (BDQ) had differing effects within each individual microenvironment (Fig. 3; Table S2).

Drug effect in caseum

In caseum, INH and BDQ had no effect on the RS ratio ($P = 0.97$ and 0.99 relative to control, respectively). By contrast, RIF10 and RIF30 reduced the RS ratio by 2.6-fold and 4.1-fold ($P = 0.04$ and 0.003 relative to control, respectively). RIF30 reduced the RS ratio

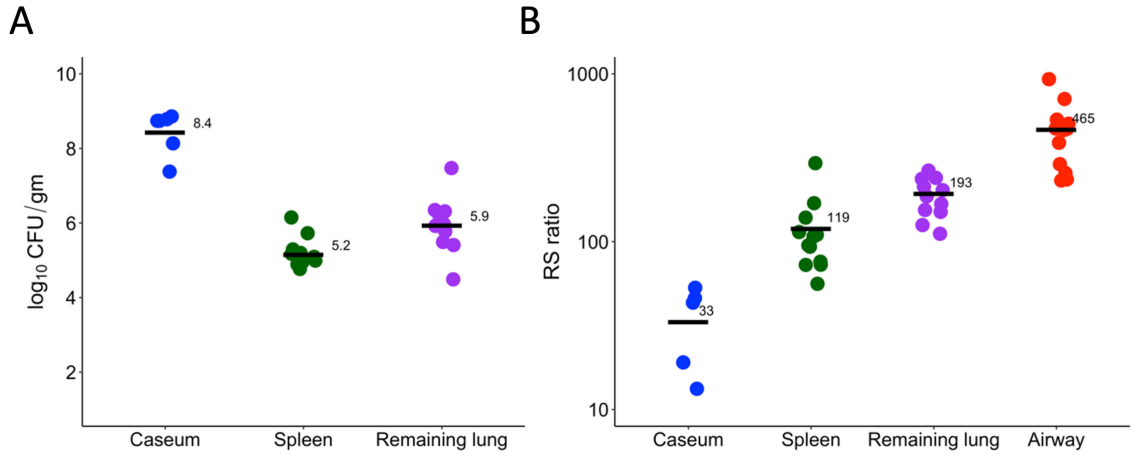

FIG 2 CFU (A) and RS ratio (B) in key microenvironments of the C3HeB/FeJ mouse prior to drug treatment. Circles represent values from individual tissue samples and horizontal bars indicate group means. Caseum, spleen, remaining lung, and airway are represented in blue, green, purple, and red, respectively. CFU is not shown for airway because BAL cannot be normalized per gram of tissue.

significantly more than INH or BDQ (P = 0.0004 and 0.001, respectively). In caseum, CFU did not identify significant differences between drugs. All drugs and doses reduced CFU in caseum by approximately one $\log_{10}$ relative to the untreated controls.

Drug effect in spleen

In the spleen, INH and RIF10 reduced the RS ratio by 5.6-fold and 9.2-fold, respectively, relative to control (minimum $P < 0.00001$). Both RIF30 and BDQ had a significantly greater effect, reducing the RS ratio at least by 20-fold relative to control (minimum $P < 0.00001$) and significantly more than INH (minimum $P < 0.00001$). In contrast to caseum where BDQ had no effect on the RS ratio, BDQ was as effective as RIF30 in the spleen ($P = 0.1$). CFU did identify significant differences between drugs in the spleen. Specifically, RIF30 or BDQ reduced CFU burdens in the spleen more than INH (minimum $P < 0.00001$) or RIF10 (minimum $P = 0.00005$).

Drug effect in remaining lung

In remaining lung, INH reduced the RS ratio by 3.5-fold relative to control ($P < 0.00001$). RIF10, RIF30, and BDQ had significantly greater effects, reducing the RS ratio by at least 15-fold relative to control (minimum $P < 0.00001$) and significantly more than INH (minimum $P =< 0.00001$). Similar to results in the spleen, BDQ was as effective as RIF30 based on the RS ratio in remaining lung ($P = 0.12$). CFU revealed significant differences between drugs in remaining lung. Specifically, RIF30 or BDQ reduced CFU burdens more than INH (minimum $P < 0.00001$) or RIF10 (minimum $P = 0.002$).

Drug effect in airway

In the airway, INH reduced the RS ratio by three-fold relative to control ($P = 0.01$). RIF10, RIF30, and BDQ had significantly greater effects, reducing the RS ratio at least by eight-fold relative to control (minimum $P < 0.00001$). RIF30 had the greatest effect in airway, reducing the RS ratio significantly more than RIF10 or BDQ (minimum $P = 0.03$). In airway, CFU did not identify significant differences between drugs. All drugs and doses reduced CFU by approximately two $\log_{10}$ relative to untreated controls in airway.

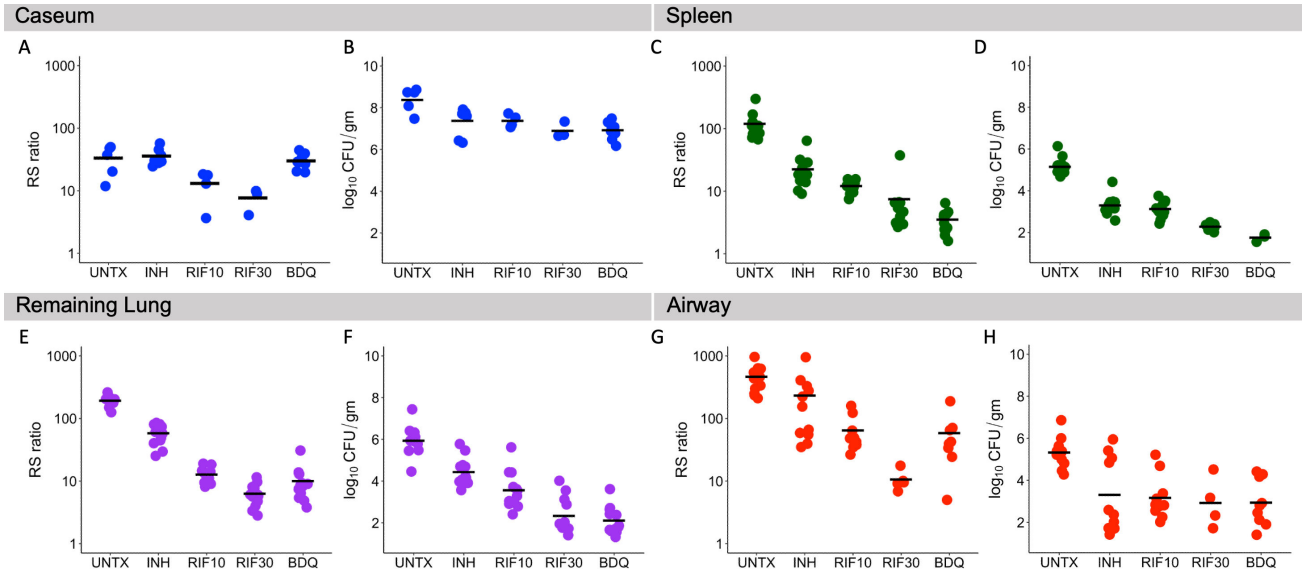

FIG 3 Effect of different drugs and doses on CFU and the RS ratio within specific microenvironments of the C3HeB/FeJ mouse. The RS ratio and CFU are shown for caseum (A and B), spleen (C and D), remaining lung (E and F), and airway (G and H). Dots indicate individual mice. Horizontal lines indicate group means. Caseum, spleen, remaining lung, and airway are represented in blue, green, purple and red, respectively.

Effects of individual drugs across different microenvironments

Using the RS ratio to evaluate individual drugs in different microenvironments revealed drug-specific changes (Fig. 4; Table S3 and S4). We evaluated both the change in RS ratio relative to control and the absolute RS ratio value following treatment.

Effect of INH in caseum, spleen, remaining lung, and airway

As noted above, INH caused a minimal change in the RS ratio relative to control in caseum (Fig. 4A). By contrast, INH reduced the RS ratio by 5.6-fold in spleen, 3.5-fold in remaining lung, and 3.0-fold in airway, representing a significantly greater reduction in all microenvironments relative to caseum (minimum $P = 0.01$). Following treatment with INH, the absolute value of the RS ratio did not differ significantly between caseum and spleen ($P = 0.3$) or remaining lung ($P = 0.5$) (Fig. 4B; Table S4). Following treatment, the RS ratio remained significantly higher in airway than in any other microenvironment (minimum $P = 0.01$). The $\log_{10}$ reduction in CFU relative to control was statistically indistinguishable between microenvironments, with the exception that CFU declined marginally more in airway than in caseum ($P = 0.04$) (Fig. 4C).

Effect of RIF10 in caseum, spleen, remaining lung and airway

RIF10 reduced the RS ratio by 2.6-fold relative to control in caseum (Fig. 4D). By contrast, RIF10 reduced the RS ratio by 9.2-fold in spleen, 15.5-fold in remaining lung, and 7.7-fold in airway, representing a significantly greater reduction in all other microenvironments than in caseum (minimum $P = 0.01$). Following treatment with RIF10, the absolute value of the RS ratio was similar in caseum, spleen, and remaining lung but remained significantly higher in airway (minimum $P < 0.00001$) (Fig. 4E; Table S4). RIF10 reduced CFU to statistically indistinguishable degrees in spleen, remaining lung, and airway (2.0 to 2.4 $\log_{10}$ CFU) (Fig. 4F). RIF10 reduced CFU significantly less in caseum than in remaining lung ($P = 0.002$) or airway ($P = 0.009$).

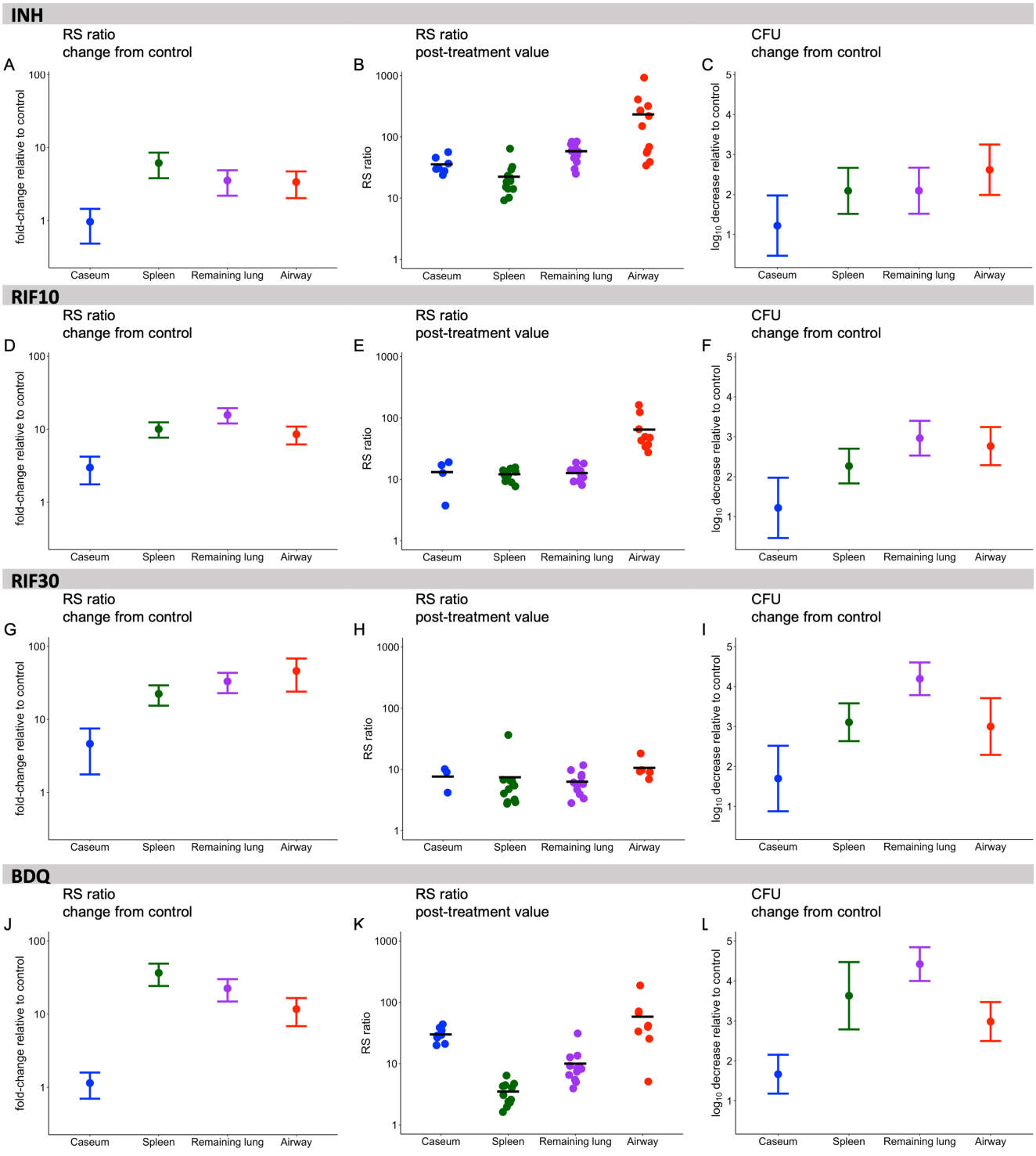

FIG 4 Effect of individual drugs and doses on the RS ratio and CFU in four microenvironments of the C3HeB/FeJ mouse. The fold change in RS ratio relative to untreated control in four microenvironments is shown for INH (A), RIF10 (D), RIF30 (G), and BDQ (J). The central dot indicates the average fold decrease in the RS ratio relative to control. Whiskers represent the 95% CI. The absolute RS ratio value following treatment is shown for INH (B), RIF10 (E), RIF30 (H), and BDQ (K). Dots indicate values from individual mice. Horizontal lines indicate group means. The change in CFU relative to control is shown for INH (C), RIF10 (F), RIF30 (I), and BDQ (L). The central dot indicates the average $\log_{10}$ decrease in CFU relative to control. Whiskers represent the 95% CI. Caseum, spleen, remaining lung, and airway are represented in blue, green, purple, and red, respectively.

Effect of RIF30 in caseum, spleen, remaining lung and airway

RIF30 reduced the RS ratio by 4.1-fold relative to control in caseum (Fig. 4G). By contrast, RIF30 reduced the RS ratio by 20.4-fold in spleen, 32.6-fold in remaining lung. and 41.7-fold in airway, representing a significantly greater reduction in all other microenvironments than in caseum (minimum $P = 0.006$). Following treatment with RIF30, the absolute value of the RS ratio was similar in all microenvironments (Fig. 4H; Table S4). RIF30 reduced CFU significantly less in caseum than in spleen ($P = 0.04$) or remaining lung ($P = 0.0001$). Evaluation of exposure response showed that RIF30 reduced the RS ratio significantly more than RIF10 in spleen, remaining lung, and airway (minimum $P = 0.004$). RIF30 also reduced CFU significantly more in spleen and remaining lung than in caseum (minimum $P = 0.002$). For caseum, there was no significant difference between RIF30 and RIF10 for either the RS ratio or CFU.

Effect of BDQ in caseum, spleen, remaining lung and airway

BDQ had minimal effect on the RS ratio in caseum (Fig. 3J). By contrast, BDQ reduced the RS ratio by 33.5-fold in spleen, 22.1-fold in remaining lung, and 10.6-fold in airway, representing a significantly greater reduction in these microenvironments than in caseum (minimum $P = 0.0008$). Following treatment with BDQ, the absolute value of the RS ratio remained significantly higher in caseum than in spleen ($P < 0.00001$) or remaining lung ($P = 0.0003$) (Fig. 3K). BDQ reduced CFU significantly less in caseum than in any other microenvironment (minimum $P = 0.004$) (Fig. 3J).

Drug distribution within microenvironments

To determine how standard potency metrics compare to concentrations achieved in each lung microenvironment and to help interpret the efficacy results, we applied drug quantitation by liquid chromatography with tandem mass spectrometry (LC/MS-MS) of samples collected by laser-capture microdissection (LCM) in thin lesion sections. Quantification of LCM samples after 17 doses demonstrated that RIF10 was present at concentrations well above the serum-shifted minimum inhibitory concentration (fMIC) (Table S5) in all sampled tissue compartments including caseum. Trough sampling 24 h after dosing showed unchanged RIF concentrations in caseum (Fig. 5A). At day 17, INH was present at concentrations well above fMIC in all sampled tissue compartments including caseum 1 h after dosing but rapidly exited, falling below fMIC after 24 h (Fig. 5B). At day 17, BDQ concentrations were similar at peak and trough and displayed a gradient in which concentrations observed in inner caseum were 16- to 28-fold lower than in the outer caseum, which showed to be proportional to the distance from the edge of the granuloma (Fig. 5C, E and F). The BDQ gradient was much more pronounced with a single dose of BDQ, wherein found levels of BDQ ranged from 1,490 ng/g (peak) to 2,465 ng/g (trough) in outer caseum to below the limit of quantification in inner caseum (Fig. 5D).

DISCUSSION

Application of the RS ratio and CFU burden demonstrated that lung microenvironments of the C3HeB/FeJ mouse harbor distinct *Mtb* phenotypes that have markedly different degrees of ongoing rRNA synthesis. Microenvironmental phenotypes appeared to be a determinant of drug effectiveness. All drugs had the lowest activity against *Mtb* populations in caseum. Even when tissue drug concentrations were above the serum-shifted MIC, certain drugs were more effective against certain microenvironmental *Mtb* populations than others. Our *in vivo* observations in C3HeB/FeJ mice support and extend results showing higher drug tolerance and differential drug activity against *Mtb* in explanted rabbit caseum *ex vivo* (3, 24). These results highlight the importance of considering PK and PD jointly. Combining a PD readout of a fundamental cellular process with lesional PK data may help to identify drugs and combinations that optimally target *Mtb* populations in caseum, a critical obstacle to shorter TB treatments.

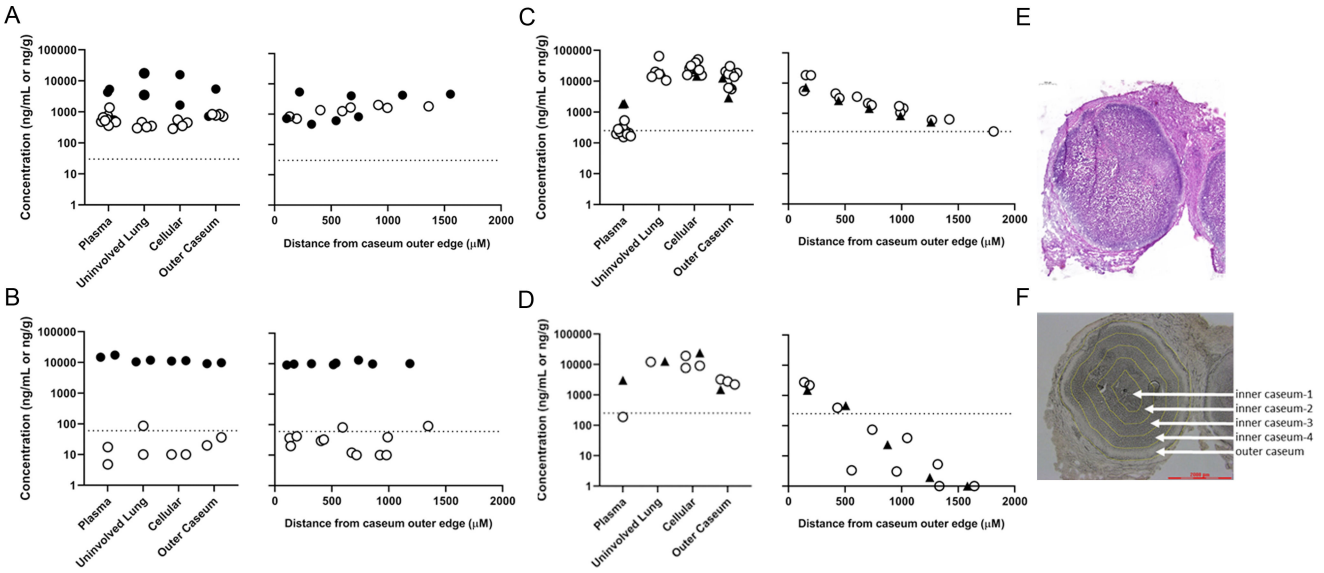

FIG 5 Drug distribution from plasma into different lung compartments, including uninvolved lung (no identifiable pathology), cellular lesions (Type III), outer caseum (foamy macrophage layer) and inner caseum (stratified by distance from inner caseum edge). (A–C) The concentration of RIF10 (A), INH (B), and BDQ (C) in caseum after 17 doses. Samples were collected from plasma and lung sections and at varying distances from the caseum outer edge at 1 h (filled circles), 5 h (filled triangles), or 24 h (open circles) after dosing. The dotted line indicates the serum-shifted MIC for each drug. (D) The concentration of BDQ in caseum after a single dose, displayed with the same formatting as in A–C. (E) Hematoxylin and eosin staining of Type I granuloma in the C3HeB/FeJ mouse. (F) Regions of the caseum were sampled by laser-capture microdissection.

Our findings are consistent with the long-standing hypothesis that one reason TB requires prolonged therapy is that unique tissue microenvironments harbor "special populations" that vary in their ability to withstand drug exposure (1, 7). The RS ratio showed that *Mtb* maintains low ongoing rRNA synthesis in caseum, indicating a quiescent slowly replicating population. This is consistent with the *ex vivo* rabbit caseum model in which CFU and chromosomal equivalents showed no evidence of *Mtb* replication (3). Indeed, our RS ratio results indicated a similarly low level of rRNA synthesis for *Mtb* in caseum *in vivo* compared to caseum surrogate *ex vivo*, which in the absence of drug treatments, is indicative of a dramatically reduced replication rate. Conversely, the *Mtb* populations of other environments appear to be replicating more quickly, with the highest RS ratios in the oxygen-rich airway.

Although caseum had a low RS ratio suggesting slow growth, caseum had a CFU burden 2.2 $\log_{10}$ higher than remaining lung. It has previously been shown that C3HeB/FeJ mice experience a phase of rapid *Mtb* replication early in granuloma development (19, 25) that is followed by slowing of replication as the lesion becomes hypoxic and necrotic (19). It is also possible that the absence of intact immune effector cells in caseum results in a decreased rate of immune elimination relative to remaining lung.

PD markers play a central role in drug evaluation because they are the readout used to assess drug effect. The historical standard PD marker is an enumeration of the burden of *Mtb* capable of growth on solid culture (*i.e.,* CFU) (26, 27). The RS ratio introduces a fundamentally different type of readout that measures a central bacterial cellular process rather than total CFU burden. The difference between RS ratio and CFU was highlighted in a recent *in vitro* analysis that showed a low correlation between drug effect on RS ratio and CFU (28). As highlighted below, this new readout of a physiologic property revealed differences in drug effects that were not discernible based on CFU, thereby providing a new perspective on the effect of individual drugs against different microenvironmental phenotypes.

INH illustrates that achieving a concentration that exceeds the fMIC is insufficient if a microenvironment harbors an *Mtb* phenotype that is capable of withstanding a drug's mechanism of action. For the quiescent *Mtb* population of caseum that likely has a low need for ongoing mycolic acid synthesis, effective concentrations of INH had no effect on the RS ratio. By contrast, for the actively replicating *Mtb* populations in spleen, remaining lung, and airway, interruption of new cell wall synthesis by INH reduced the RS ratio by 3.0- to 5.6-fold. This is consistent with a body of evidence showing that INH is effective primarily against replicating *Mtb,* with minimal activity against nonreplicating *Mtb* (3, 29, 30). In contrast to the RS ratio, CFU did not reveal differences between the effect of INH in different microenvironments, with the exception that CFU declined marginally more in airway than caseum. INH highlights the importance of bacterial phenotype and the information provided by a new molecular marker of rRNA synthesis.

RIF reduced the RS ratio in all sampled tissue compartments, indicating that RIF has activity against the phenotypes found in all microenvironments. Because there has long been uncertainty about optimal rifampin dosing (31, 32), we tested the human-equivalent standard dose (10 mg/kg) as well as a human-relevant higher dose (30 mg/kg). Consistent with evidence that higher-dose rifampin has greater activity in preclinical animals and humans (33), RIF10 and RIF30 demonstrated a strong dose–response relationship in spleen, remaining lung, and airway. Nonetheless, both RS ratio and CFU indicated that RIF was less effective in caseum than in any other microenvironment. This highlights that caseum phenotypes are better able to tolerate even high concentrations of RIF, the prototypical sterilizing agent that is the backbone of existing front-line TB treatment.

BDQ represents a different example. In microenvironments that achieved high BDQ concentrations (*e.g.,* remaining lung), BDQ matched the potency of RIF30 as measured by RS ratio and CFU. By contrast, drug distribution of BDQ into caseum appeared to be proportional to the number of doses administered and inversely correlated with distance from the outer caseum edge. Spatial drug distribution studies by LCM LC/MS-MS suggested that after 2.5 wk of treatment the concentration of BDQ ranged from 14.6 μg/g in outer caseum to as low as 0.25 μg/g in inner caseum and the effect on RS ratio was correspondingly negligible. Comparing the concentration gradient after 1 and 17 doses (Fig. 5C and D) suggests that BDQ slowly penetrates avascular caseum and may not have reached steady state at the 2.5 wk mark, consistent with the slow onset of efficacy in an early bactericidal activity Phase II trial (34). The current results do not indicate what the effect of BDQ might be were adequate caseum concentrations achieved.

Our observation that all drugs have diminished effectiveness in C3HeB/FeJ mouse caseum is broadly consistent with previous results from the rabbit *ex vivo* caseum model (3). Using CFU as a readout, Sarathy *et.al.* found that the caseum minimum bactericidal concentration of first- and second-line drugs was higher in rabbit caseum than under standard *in vitro* conditions with replicating cultures. Because the RS ratio is a direct molecular PD readout that does not require confounding steps such as recovery and outgrowth of bacteria, the RS ratio enabled this first comparison of phenotypes and drug effects across tissue microenvironments. The RS ratio extends and complements results from the *ex vivo* rabbit caseum model by measuring a fundamental cellular process rather than bacillary burden.

In contrast to our results, a recent manuscript that evaluated a fluorescent reporter *Mtb* strain in C3HeB/FeJ mouse lesions reported that *Mtb* was more actively replicating in the caseum core than in the cuff, and the *Mtb* population of the core showed greater susceptibility to INH (25). Importantly, the previous report evaluated a different timepoint than tested here. Lavin and Tan (25) evaluated mice 6 wk post-infection (a timepoint at which previous studies would suggest lesions are in the maturation process (19)) and identified rapidly replicating caseum phenotypes that were highly susceptible to INH. By contrast, we evaluated mice starting treatment at 10 wk post-infection (a timepoint at which lesions are mature and well encapsulated with high *Mtb* burden) and

identified slowly replicating caseum phenotypes that were INH tolerant. In combination, these observations appear to highlight how the evolution of lesions and phenotypes over time dictates drug effectiveness. Time-course studies using a single consistent assay method are needed to confirm this hypothesis.

This report has several limitations. This proof-of-concept study included limited PK measurements that were insufficient for statistical pharmacokinetic modeling. Future studies can maximize the value of lesional analysis by pairing lesional PD (based on RS ratio and CFU) with comprehensive lesional PK profiles. Second, the RS ratio provides a snapshot of average rRNA synthesis across an entire *Mtb* population. Using *in situ* hybridization with single-bacillary resolution, we have previously shown that caseum harbors multiple *Mtb* phenotypes with differing degrees of ongoing rRNA synthesis (8, 15). In future studies, the joint PK/PD evaluation demonstrated here can be extended with even more spatially granular methods.

This study has shown that different tissue microenvironments harbor phenotypically distinct *Mtb* populations that respond to drug treatment differently. As a molecular readout of a fundamental cellular process, the RS ratio provides a new metric for evaluating efficacy in lesions that does not rely on bacillary burden. This report points to a new era in which lesional PK can be combined with molecular assays of bacterial cellular processes like the RS ratio to design regimens that optimally target caseum phenotypes and achieve the end goal of shorter, more effective TB treatments.

MATERIALS AND METHODS

Drug susceptibility profiling

The minimum inhibitory concentration (MIC) was determined for RIF, INH, and BDQ against *Mtb* Erdman in 7H9 media supplemented with 0.2% [vol:vol] of glycerol and 10% [vol:vol] of albumin-dextrose-catalase (ADC), with 0.05% [vol:vol] of Tween-80 (7H9 media). MICs were determined by a broth microdilution assay using two-fold serial drug dilutions. The lowest consecutive antimicrobial concentration that showed a ≥80% reduction in OD_{600} relative to drug-free control wells was regarded as the MIC. In parallel, the MICs were also determined in the presence of 4% (wt/vol) of human serum albumin (Sigma # A1653) which is defined here as the serum-shifted MIC.

Animals

Female-specific pathogen-free C3HeB/FeJ mice, aged 8–10 weeks, were purchased from Jackson Laboratories (Bar Harbor, ME). Mice were housed in an animal bio-safety level III (ABSL-3) facility employing autoclaved bedding, water, and mouse chow *ad libitum*. All procedures were approved by Colorado State University Institutional Animal Care and Use Committee (IACUC) (Reference numbers of approved protocol: KP 1515).

Aerosol infection

C3HeB/FeJ mice were exposed to a low-dose aerosol infection with the *Mtb* Erdman strain (TMCC 107) using a Glas-Col inhalation exposure system resulting in an average of 50–75 bacteria in lungs 1 d following aerosol (8, 35). Infected mice were observed and weighed at least once a week. Starting from day 21 until the start of therapy, mice were observed and weighed two to three times per week, due to the increased incidence of morbidity and mortality associated with clinical TB disease. Any mice exhibiting clinical symptoms of illness were humanely euthanized.

Drug preparation and drug treatment

Rifampin (Sigma) and isoniazid (Sigma) were dissolved in sterile water. Bedaquiline fumarate (PharmaBlock) was dissolved in 20% (wt/vol) of 2-hydroxypropyl-β-cyclodextrin and formulated as described previously (36, 37). For drug efficacy experiments, C3HeB/FeJ mice were randomized (n = 12 per group) and dosed once daily starting

10 wk post-aerosol with rifampin at 10 mg/kg or 30 mg/kg, isoniazid at 25 mg/kg, or bedaquiline fumarate at 25 mg/kg, 7 d per week by oral gavage in 0.2 mL of volume for the total number of doses indicated.

Histological analysis

A separate group of mice were sacrificed and whole lungs were fixed for histopathology purposes. Lung perfusions were performed by clamping the caudal vena cava with straight-tipped hemostats and cutting the vena cava between the hemostats and the liver to allow blood to drain. A 24-guage 0.75-inch catheter was inserted into the right ventricle of the heart and blood was flushed using phosphate-buffered saline (PBS) with 0.04% [wt:vol] of ethylenediaminetetraacetic acid followed by 10 mL of 4% paraformaldehyde (PFA). Lungs were recovered and placed into a histology cassette and incubated for 48 h in 4% of PFA for 48 h prior to transfer to PBS. Lungs were sectioned and stained with hematoxylin–eosin (H&E).

Collection of samples for bacterial enumeration and RS ratio

Each mouse was individually euthanized by CO_2 narcosis followed by cardiac puncture. Airway was sampled by BAL by passing a total of 2.5 mL of PBS into the lungs through a 24-guage 0.75-inch catheter inserted into the trachea. An amount of 0.5 mL of BAL was used for CFU enumeration, and an amount of 0.5 mL was placed into 2 mL of CAMM-RPS buffer to preserve RNA. The remaining BAL was collected by cytospin for Wright's Giemsa staining. Spleens were aseptically collected. Lungs were recovered, photographed, and diagramed. To collect inner caseum and avoid cross-contamination from the granuloma's cellular cuff, we first identified lung lobes featuring large encapsulated caseous necrotic granulomas (Type I). The granuloma capsule was carefully incised with a scalpel and the granuloma sides were gently squeezed with tweezers to open the incision and expose the inner caseum. A small spoon was inserted through the incision and used to scoop out a small amount (~0.01 to 0.03 g) of the inner caseum which was split to two cryovials. All tissue samples were divided in half and weights were recorded. Samples were flash-frozen in liquid nitrogen and stored at −80°C prior to further processing.

Tissues were disrupted with a tissue homogenizer (Precellys, Bertin Instruments, Rockville, MD) in PBS plus 10% [wt/vol] of bovine serum albumin for CFU enumeration on 7H11 agar further supplemented with 0.4% activated charcoal to prevent drug carry-over as described previously (15). Colonies were enumerated after at least 28 d of incubation at 37°C and the plates were incubated for 8 wk to ensure that all viable colonies were detected. For RNA extraction, tissues were homogenized in Trizol (15).

Caseum surrogate model

PMA-differentiated THP-1 macrophages were infected with irradiated *Mtb* (BEI Resources) at an approximate multiplicity of infection of 1:50. Foamy macrophages were washed three times with PBS, followed by three freeze–thaw cycles to lyse the cells and incubated at 75°C for 20 min to denature proteins in the matrix. The caseum surrogate matrix was rested for 3 d at 37°C and stored at −20°C prior to inoculation.

Collection of samples from caseum surrogate

Mtb HN878 grown to mid-log phase in 7H9 media was harvested by centrifugation, suspended in sterile water, and inoculated into the caseum surrogate (22, 23) at 10^8 CFU/mL. The inoculated caseum surrogate was mixed briefly using 1.4 mm zirconium oxide beads (CK14 soft tissue; Precellys, Bertin Instruments, Rockville, MD) to achieve a homogeneous suspension. After 8-wk incubation in a sealed tube at 37°C to allow for physiologic and metabolic adaptation to the lipid-rich environment, CAMM-RPS buffer was added at 3 × the total caseum surrogate volume to preserve RNA.

Collection of samples for pharmacokinetic analysis

For the PK experiments, 9–10 C3HeB/FeJ mice were dosed starting 10 wk post-aerosol as described above. Treatment occurred 7 d per week for up to a total of 17 doses. Drugs were prepared as described above for the efficacy studies. Mice were euthanized, and plasma and tissues were collected at two timepoints, selected based on the plasma C_{max} (1 or 5 h) and C_{min} (24 h). Whole blood was obtained via cardiac puncture and processed in plasma separator tubes (Becton, Dickinson and Co., Franklin Lakes, NJ, USA) and centrifuged at 3,000 × relative centrifugal force for 2 min at 4°C, aliquoted into Eppendorf microcentrifuge tubes and stored at −80°C until analysis. Mice with pronounced lung pathology were selected to collect samples for spatial drug quantitation by gravity-assisted LCM. Briefly, whole lung samples were collected on clear disposable base molds (Fisher Scientific, Hampton, NH, USA). Using forceps, tissues were collected on trays placed on a prechilled aluminum block held in liquid nitrogen, and frozen within 1–2 min. Tissue trays containing frozen lobes were wrapped in foil squares, placed individually into labeled zip-lock bags, and immediately transferred onto dry ice.

Drug quantitation by HPLC coupled to tandem mass spectrometry (LC/MS-MS)

Drug levels in tissue were determined by spatial quantitation in thin tissue sections by LCM followed by LC/MS-MS analysis of microdissected areas (38). The benefit of the LCM approach is the ability to obtain absolute drug levels in defined areas of Type I lung lesions such as caseum (the core of the caseous necrotic lesion) without cross-contamination. The tissue sections of 25 µm thickness were cut from infected mouse lung biopsies using a Leica CM 1860UV (Buffalo Grove, IL) and thaw-mounted onto Leica PET-Membrane FrameSlides (Buffalo Grove, IL) of 1.4 µm thickness. Approximately 10 µm thick tissue sections were thaw-mounted onto standard glass microscopy slides for H&E staining. Sequential rings of necrotic tissue proceeding from the border with the cellular rim to the core of the caseous compartment were demarcated for each tissue section by creating a mask of caseum and processing it using the Exact Euclidean Distance Transform plugin in ImageJ (National Institutes of Health, MD). Sequential rings of necrotic tissue were then dissected using a Leica LMD6 system (Buffalo Grove, IL). Dissected lesion tissues were collected into standard PCR tubes of 0.25 mL and immediately transferred to −80°C.

RIF, BDQ, INH, and verapamil (VER) were purchased from Sigma Aldrich (St. Louis, MO, USA); RIF-d8, BDQ-d6, and INH-d4 were purchased from Toronto Research Chemicals (Ontario). Drug-free lung and K_2EDTA plasma from CD-1 mice was obtained from BioIVT (Westbury, NY) for use as blank matrices to build standard curves. Neat 1 mg/mL dimethyl sulfoxide stocks were serially diluted in 50:50 acetonitrile/water to create a standard curve and quality control spiking solutions and 10 µL of neat spiking solutions were added to 2 µL of lesion homogenate prior to extraction. On the day of analysis, samples were extracted by adding 50 µL of extraction solution (acetonitrile/methanol, 1:1) containing 1, 10, 4, and 5 ng/mL of VER, INH-d4, RIF-d8, and BDQ-d6, respectively. Extracts were sonicated for 5 min and centrifuged at 10,000 rpm for 5 min, and 40 µL of supernatant was transferred to 96-well deep plates for LC-MS/MS analysis. For INH quantitation, 40 µL of 2% cinnamaldehyde in methanol was added to derivatize isoniazid prior to analysis. For RIF quantitation, 5 µl of 75 mg/mL ascorbic acid was added to extracts to stabilize RIF during analysis.

LC/MS-MS analysis was performed on a Sciex Qtrap 6500 + triple-quadrupole mass spectrometer coupled to a Shimadzu Nexera X2 UHPLC system. Chromatography was performed on an Agilent Zorbax SB-C8 column (2.1 × 30 mm; particle size 3.5 µm) using a reverse phase gradient. Deionized water with 0.1% formic acid (FA) was used for the aqueous mobile phase and 0.1% FA in acetonitrile for the organic mobile phase. Multiple-reaction monitoring (MRM) of precursor/fragment transitions in the electrospray positive-ionization mode was used to quantify the analytes. MRM transitions of 823.30/791.30, 555.00/58.00, 252.200/80.30 455.40/165.20, 831.30/799.40, 561.00/64.00,

and 256.20/84.30 were used for RIF, BDQ, INH, VER, RIF-d8, BDQ-d6, and INH-d4, respectively. Data processing was performed using Analyst software version 1.6.3 (Sciex).

RNA extraction and RS ratio profiling

RNA was extracted from tissue and BAL samples after homogenization in Trizol (15). Briefly, eukaryotic cellular debris was pelleted and the lysate was mixed with chloroform. A solution of 50% isopropanol, 0.8M sodium citrate, and 1.2M sodium chloride was mixed with the aqueous phase and nucleic acids were precipitated overnight at 4°C. Nucleic acids were pelleted by centrifugation, washed twice with 70% ethanol, and resuspended in water. DNA was digested in a multi-step process, with the initial digestion performed using two additions of Promega RQ1 DNase followed by a 15-min incubation at 37°C after each DNase addition. RNA was further purified and DNA was digested on a Maxwell RSC instrument (Promega) with the Maxwell RSC simplyRNA tissue kit. Purification was performed following the manufacturer's instructions, with DNase added at twice the recommended amount.

Purified RNA was reverse transcribed to cDNA using SuperScript III VILO cDNA synthesis kit (Invitrogen) at 42°C for 120 min. The RS ratio was measured by quantification of ETS1 and 23S rRNA gene transcripts in the cDNA using droplet digital PCR in a duplexed reaction. Droplet digital PCRs were performed using the QX200 Droplet Digital PCR system with ddPCR SuperMix for Probes (no dUTP) (Bio-Rad). The RS ratio was calculated from each duplexed reaction by the QX200 Droplet Digital PCR system software (QuantaSoft AP, Bio-Rad).

Statistical analysis

A one-way ANOVA was performed to compare the effect of different drugs or microenvironments on CFU and the RS ratio followed by a multiple comparison analysis of variance using a one-way Tukey test. Differences were considered significant at the 95% confidence level ($P < 0.05$). Data management, plotting, and post-modeling analysis were conducted using R (v 4.2.1; R Development Core Team, Vienna, Austria).

ACKNOWLEDGMENTS

N.D.W. acknowledges funding from Veterans Affairs (1I01B × 004527–01A1) and the US National Institutes of Health (1R01AI127300-01A1). N.D.W. and M.I.V. acknowledge funding from the US National Institutes of Health (1R21AI135652-01). N.D.W., M.I.V., G.T.R., and R.M.S. acknowledge funding from the Bill & Melinda Gates Foundation (OPP1213947). G.T.R., N.D.W., and V.D. acknowledge funding from the Bill & Melinda Gates Foundation (OPP1126594).

N.D.W., G.T.R., R.M.S., M.I.V., and B.K.P. conceived of the project and planned the experiments. N.D.W. and G.T.R. drafted the manuscript. A.A.B., M.E.R., and L.M.M. conducted the animal experiments. K.R., S.P., and R.A.M. performed the molecular assays. F.K. and J.P.S. performed the PK analyses. C.D.A., M.D.Z., J.P.E., and V.D. analyzed the molecular and PK results.

AUTHOR AFFILIATIONS

[1]Rocky Mountain Regional VA Medical Center, Aurora, Colorado, USA
[2]Division of Pulmonary Sciences and Critical Care Medicine, University of Colorado Anschutz Medical Campus, Aurora, Colorado, USA
[3]Consortium for Applied Microbial Metrics, Aurora, Colorado, USA
[4]Department of Bioengineering and Therapeutic Sciences, University of California San Francisco, San Francisco, California, USA
[5]Mycobacteria Research Laboratories, Department of Microbiology, Immunology and Pathology, Colorado State University, Fort Collins, Colorado, USA
[6]Department of Immunology and Microbiology, University of Colorado Anschutz Medical Campus, Aurora, Colorado, USA

[7]Center for Discovery and Innovation, Nutley, New Jersey, USA

AUTHOR ORCIDs

Véronique Dartois http://orcid.org/0000-0001-9470-5009
Radojka M. Savic http://orcid.org/0000-0003-3143-5579
Gregory T. Robertson http://orcid.org/0000-0001-7157-4034

FUNDING

Funder	Grant(s)	Author(s)
U.S. Department of Veterans Affairs (VA)	1I01BX004527-01A1	Nicholas D. Walter
HHS | National Institutes of Health (NIH)	1R01AI127300-01A1	Nicholas D. Walter
HHS | National Institutes of Health (NIH)	1R21AI135652-01	Martin I. Voskuil Nicholas D. Walter
Bill and Melinda Gates Foundation (GF)	OPP1213947	Gregory Thomas Robertson Nicholas D. Walter Martin I. Voskuil Radojka M. Savic
Bill and Melinda Gates Foundation (GF)	OPP1126594	Nicholas D Walter Veronique Dartois Gregory T. Robertson

AUTHOR CONTRIBUTIONS

Michelle E. Ramey, Investigation.

ADDITIONAL FILES

The following material is available online.

Supplemental Material

Tables S1 to S5 (AAC00284-23-s0001.docx). Supplemental results.

REFERENCES

1. Connolly LE, Edelstein PH, Ramakrishnan L. 2007. Why is long-term therapy required to cure tuberculosis? PLoS Med 4:e120. https://doi.org/10.1371/journal.pmed.0040120
2. Lenaerts A, Barry CE, Dartois V. 2015. Heterogeneity in tuberculosis pathology, microenvironments and therapeutic responses. Immunol Rev 264:288–307. https://doi.org/10.1111/imr.12252
3. Sarathy JP, Via LE, Weiner D, Blanc L, Boshoff H, Eugenin EA, Barry CE, Dartois VA. 2018. Extreme drug tolerance of *Mycobacterium tuberculosis* in caseum. Antimicrob Agents Chemother 62:e02266-17. https://doi.org/10.1128/AAC.02266-17
4. Strydom N, Gupta SV, Fox WS, Via LE, Bang H, Lee M, Eum S, Shim T, Barry CE, Zimmerman M, Dartois V, Savic RM. 2019. Tuberculosis drugs' distribution and emergence of resistance in patient's lung lesions: a mechanistic model and tool for regimen and dose optimization. PLoS Med 16:e1002773. https://doi.org/10.1371/journal.pmed.1002773
5. Irwin SM, Prideaux B, Lyon ER, Zimmerman MD, Brooks EJ, Schrupp CA, Chen C, Reichlen MJ, Asay BC, Voskuil MI, Nuermberger EL, Andries K, Lyons MA, Dartois V, Lenaerts AJ. 2016. Bedaquiline and pyrazinamide treatment responses are affected by pulmonary lesion heterogeneity in *Mycobacterium tuberculosis* infected C3HeB/FeJ. ACS Infect Dis 2:251–267. https://doi.org/10.1021/acsinfecdis.5b00127
6. Prideaux B, Via LE, Zimmerman MD, Eum S, Sarathy J, O'Brien P, Chen C, Kaya F, Weiner DM, Chen P-Y, Song T, Lee M, Shim TS, Cho JS, Kim W, Cho SN, Olivier KN, Barry CE, Dartois V. 2015. The association between sterilizing activity and drug distribution into tuberculosis lesions. Nat Med 21:1223–1227. https://doi.org/10.1038/nm.3937
7. Mitchison DA. 1979. Basic mechanisms of chemotherapy. Chest 76:771–781. https://doi.org/10.1378/chest.76.6_supplement.771
8. Robertson GT, Ramey ME, Massoudi LM, Carter CL, Zimmerman M, Kaya F, Graham BG, Gruppo V, Hastings C, Woolhiser LK, Scott DWL, Asay BC, Eshun-Wilson F, Maidj E, Podell BK, Vásquez JJ, Lyons MA, Dartois V, Lenaerts AJ. 2021. Comparative analysis of pharmacodynamics in the C3HeB/FeJ mouse tuberculosis model for DprE1 inhibitors TBA-7371, PBTZ169 and OPC-167832. Antimicrob Agents Chemother 65:e0058321. https://doi.org/10.1128/AAC.00583-21
9. Ernest JP, Sarathy J, Wang N, Kaya F, Zimmerman MD, Strydom N, Wang H, Xie M, Gengenbacher M, Via LE, Barry CE, Carter CL, Savic RM, Dartois V. 2021. Lesion penetration and activity limit the utility of second-line injectable agents in pulmonary tuberculosis. Antimicrob Agents Chemother 65:e0050621. https://doi.org/10.1128/AAC.00506-21
10. Bumann D. 2015. Heterogeneous host-pathogen encounters: act locally, think globally. Cell Host Microbe 17:13–19. https://doi.org/10.1016/j.chom.2014.12.006

11. Santucci P, Greenwood DJ, Fearns A, Chen K, Jiang H, Gutierrez MG. 2021. Intracellular localisation of *Mycobacterium tuberculosis* affects efficacy of the antibiotic pyrazinamide. Nat Commun 12:3816. https://doi.org/10.1038/s41467-021-24127-3
12. Barry CE, Boshoff HI, Dartois V, Dick T, Ehrt S, Flynn J, Schnappinger D, Wilkinson RJ, Young D. 2009. The spectrum of latent tuberculosis: rethinking the biology and intervention strategies. Nat Rev Microbiol 7:845–855. https://doi.org/10.1038/nrmicro2236
13. Mattila JT, Ojo OO, Kepka-Lenhart D, Marino S, Kim JH, Eum SY, Via LE, Barry CE, Klein E, Kirschner DE, Morris SM, Lin PL, Flynn JL. 2013. Microenvironments in tuberculous granulomas are delineated by distinct populations of macrophage subsets and expression of nitric oxide synthase and arginase isoforms. J Immunol 191:773–784. https://doi.org/10.4049/jimmunol.1300113
14. Lin PL, Ford CB, Coleman MT, Myers AJ, Gawande R, Ioerger T, Sacchettini J, Fortune SM, Flynn JL. 2014. Sterilization of granulomas is common in active and latent tuberculosis despite within-host variability in bacterial killing. Nat Med 20:75–79. https://doi.org/10.1038/nm.3412
15. Walter ND, Born SEM, Robertson GT, Reichlen M, Dide-Agossou C, Ektnitphong VA, Rossmassler K, Ramey ME, Bauman AA, Ozols V, Bearrows SC, Schoolnik G, Dolganov G, Garcia B, Musisi E, Worodria W, Huang L, Davis JL, Nguyen NV, Nguyen HV, Nguyen ATV, Phan H, Wilusz C, Podell BK, Sanoussi ND, de Jong BC, Merle CS, Affolabi D, McIlleron H, Garcia-Cremades M, Maidji E, Eshun-Wilson F, Aguilar-Rodriguez B, Karthikeyan D, Mdluli K, Bansbach C, Lenaerts AJ, Savic RM, Nahid P, Vásquez JJ, Voskuil MI. 2021. *Mycobacterium tuberculosis* precursor rRNA as a measure of treatment-shortening activity of drugs and regimens. Nat Commun 12:2899. https://doi.org/10.1038/s41467-021-22833-6
16. Gourse RL, Gaal T, Bartlett MS, Appleman JA, Ross W. 1996. rRNA transcription and growth rate-dependent regulation of ribosome synthesis in *Escherichia coli*. Annu Rev Microbiol 50:645–677. https://doi.org/10.1146/annurev.micro.50.1.645
17. Maitra A, Dill KA. 2015. Bacterial growth laws reflect the evolutionary importance of energy efficiency. Proc Natl Acad Sci U S A 112:406–411. https://doi.org/10.1073/pnas.1421138111
18. Driver ER, Ryan GJ, Hoff DR, Irwin SM, Basaraba RJ, Kramnik I, Lenaerts AJ. 2012. Evaluation of a mouse model of necrotic granuloma formation using C3HeB/FeJ mice for testing of drugs against *Mycobacterium tuberculosis*. Antimicrob Agents Chemother 56:3181–3195. https://doi.org/10.1128/AAC.00217-12
19. Irwin SM, Driver E, Lyon E, Schrupp C, Ryan G, Gonzalez-Juarrero M, Basaraba RJ, Nuermberger EL, Lenaerts AJ. 2015. Presence of multiple lesion types displaying vastly different microenvironments in C3HeB/FeJ mice following aerosol infection with *M. tuberculosis*. Dis Model Mech 8:591–602. https://doi.org/10.1242/dmm.019570
20. Sarathy JP, Xie M, Jones RM, Chang A, Osiecki P, Weiner D, Tsao W-S, Dougher M, Blanc L, Fotouhi N, Via LE, Barry CE, De Vlaminck I, Sherman DR, Dartois VA. 2023. A novel tool to identify bactericidal compounds against vulnerable targets in drug-tolerant *M. tuberculosis* found in caseum. mBio 14:e0059823. https://doi.org/10.1128/mbio.00598-23
21. Sarathy JP, Liang H-P, Weiner D, Gonzales J, Via LE, Dartois V. 2017. An *in vitro* caseum binding assay that predicts drug penetration in tuberculosis lesions. J Vis Exp:55559. https://doi.org/10.3791/55559
22. Sarathy JP, Zuccotto F, Hsinpin H, Sandberg L, Via LE, Marriner GA, Masquelin T, Wyatt P, Ray P, Dartois V. 2016. Prediction of drug penetration in tuberculosis lesions. ACS Infect Dis 2:552–563. https://doi.org/10.1021/acsinfecdis.6b00051
23. Kreutzfeldt KM, Jansen RS, Hartman TE, Gouzy A, Wang R, Krieger IV, Zimmerman MD, Gengenbacher M, Sarathy JP, Xie M, Dartois V, Sacchettini JC, Rhee KY, Schnappinger D, Ehrt S. 2022. Cina mediates multidrug tolerance in *Mycobacterium tuberculosis*. Nat Commun 13:2203. https://doi.org/10.1038/s41467-022-29832-1
24. Sarathy JP, Dartois V. 2020. Caseum: a niche for *Mycobacterium tuberculosis* drug-tolerant persisters. Clin Microbiol Rev 33:e00159-19. https://doi.org/10.1128/CMR.00159-19
25. Lavin RC, Tan S. 2022. Spatial relationships of intra-lesion heterogeneity in *Mycobacterium tuberculosis* microenvironment, replication status, and drug efficacy. PLoS Pathog 18:e1010459. https://doi.org/10.1371/journal.ppat.1010459
26. Dooley KE, Phillips PPJ, Nahid P, Hoelscher M. 2016. Challenges in the clinical assessment of novel tuberculosis drugs. Adv Drug Deliv Rev 102:116–122. https://doi.org/10.1016/j.addr.2016.01.014
27. Gumbo T, Lenaerts AJ, Hanna D, Romero K, Nuermberger E. 2015. Nonclinical models for antituberculosis drug development: a landscape analysis. J Infect Dis 211:S83–S95. https://doi.org/10.1093/infdis/jiv183
28. Reichlen MJ, Born SEM, Lyons MA, Rossmassler K, Reid J, Robertson GT, Walter ND, Voskuil MI. 2023. Standardized RS ratio metrics to assess tuberculosis antimicrobial efficacy and potency. Antimicrob Agents Chemother 67:e0148322. https://doi.org/10.1128/aac.01483-22
29. Karakousis PC, Williams EP, Bishai WR. 2008. Altered expression of isoniazid-regulated genes in drug-treated dormant *Mycobacterium tuberculosis*. J Antimicrob Chemother 61:323–331. https://doi.org/10.1093/jac/dkm485
30. Ahmad Z, Klinkenberg LG, Pinn ML, Fraig MM, Peloquin CA, Bishai WR, Nuermberger EL, Grosset JH, Karakousis PC. 2009. Biphasic kill curve of isoniazid reveals the presence of drug-tolerant, not drug-resistant, *Mycobacterium tuberculosis* in the guinea pig. J Infect Dis 200:1136–1143. https://doi.org/10.1086/605605
31. van Ingen J, Aarnoutse RE, Donald PR, Diacon AH, Dawson R, Plemper van Balen G, Gillespie SH, Boeree MJ. 2011. Why do we use 600 mg of rifampicin in tuberculosis treatment? Clin Infect Dis 52:e194–e199. https://doi.org/10.1093/cid/cir184
32. Grobbelaar M, Louw GE, Sampson SL, van Helden PD, Donald PR, Warren RM. 2019. Evolution of rifampicin treatment for tuberculosis. Infect Genet Evol 74:103937. https://doi.org/10.1016/j.meegid.2019.103937
33. Svensson RJ, Svensson EM, Aarnoutse RE, Diacon AH, Dawson R, Gillespie SH, Moodley M, Boeree MJ, Simonsson USH. 2018. Greater early bactericidal activity at higher rifampicin doses revealed by modeling and clinical trial simulations. J Infect Dis 218:991–999. https://doi.org/10.1093/infdis/jiy242
34. Rustomjee R, Diacon AH, Allen J, Venter A, Reddy C, Patientia RF, Mthiyane TCP, De Marez T, van Heeswijk R, Kerstens R, Koul A, De Beule K, Donald PR, McNeeley DF. 2008. Early bactericidal activity and pharmacokinetics of the diarylquinoline TMC207 in treatment of pulmonary tuberculosis. Antimicrob Agents Chemother 52:2831–2835. https://doi.org/10.1128/AAC.01204-07
35. Kelly BP, Furney SK, Jessen MT, Orme IM. 1996. Low-dose aerosol infection model for testing drugs for efficacy against *Mycobacterium tuberculosis*. Antimicrob Agents Chemother 40:2809–2812. https://doi.org/10.1128/AAC.40.12.2809
36. Andries K, Verhasselt P, Guillemont J, Göhlmann HWH, Neefs J-M, Winkler H, Van Gestel J, Timmerman P, Zhu M, Lee E, Williams P, de Chaffoy D, Huitric E, Hoffner S, Cambau E, Truffot-Pernot C, Lounis N, Jarlier V. 2005. A diarylquinoline drug active on the ATP synthase of *Mycobacterium tuberculosis*. Science 307:223–227. https://doi.org/10.1126/science.1106753
37. Hoff DR, Ryan GJ, Driver ER, Ssemakulu CC, De Groote MA, Basaraba RJ, Lenaerts AJ. 2011. Location of intra- and extracellular *M. tuberculosis* populations in lungs of mice and guinea pigs during disease progression and after drug treatment. PLoS One 6:e17550. https://doi.org/10.1371/journal.pone.0017550
38. Zimmerman M, Blanc L, Chen P-Y, Dartois V, Prideaux B. 2018. Spatial quantification of drugs in pulmonary tuberculosis lesions by laser capture microdissection liquid chromatography mass spectrometry (LCM-LC/MS). J Vis Exp:57402. https://doi.org/10.3791/57402